Draft version March 15, 2016
Preprint typeset using LaTeX style emulateapj v. 5/2/11

arXiv:1602.02774v2 [astro-ph.HE] 13 Mar 2016

TYPE II SUPERNOVAE PROGENITOR AND EJECTA PROPERTIES FROM THE TOTAL EMITTED LIGHT, *ET*

Tomer Shussman[1], Ehud Nakar[1], Roni Waldman [2,3], Boaz Katz[3]

Draft version March 15, 2016

ABSTRACT

It was recently shown that the bolometric light curves of type II supernovae (SNe) allow an accurate and robust measurement of the product of the radiation energy in the ejecta, E_r, and the time since the explosion, t, at early phases ($t \lesssim 10d$) of the homologous expansion. This observable, denoted here $ET \equiv E_r t$ is constant during that time and depends only on the progenitor structure and explosion energy. We use a 1D hydrodynamic code to find ET of simulated explosions of 145 red supergiant progenitors obtained using the stellar evolution code MESA, and relate this observable to the properties of the progenitor and the explosion energy. We show that ET probes only the properties of the envelope (velocity, mass and initial structure), similarly to other observables that rely on the photospheric phase emission. Nevertheless, for explosions where the envelope dominates the ejected mass, $M_{\rm env}/M_{\rm ej} \gtrsim 0.6$, ET is directly related to the explosion energy $E_{\rm exp}$ and ejected mass $M_{\rm ej}$ through the relation $ET \approx 0.15 E_{\rm exp}^{1/2} R_* M_{\rm ej}^{1/2}$, where R_* is the progenitor radius, to an accuracy better than 30%. We also provide relations between ET and the envelope properties that are accurate (to within 20%) for all the progenitors in our sample, including those that lost most of their envelope. We show that when the envelope velocity can be reasonably measured by line shifts in observed spectra, the envelope is directly constrained from the bolometric light curve (independent of $E_{\rm exp}$). We use that to compare observations of 11 SNe with measured ET and envelope velocity to our sample of numerical progenitors. This comparison suggests that many SNe progenitors have radii that are $\lesssim 500\ R_\odot$. In the framework of our simulations this indicates, most likely, a rather high value of the mixing length parameter.

Subject headings: Type II supernovae

1. INTRODUCTION

The most common type of supernovae (SNe) are type II supernovae (supernovae with spectra showing significant amounts of hydrogen) and yet it is still unclear how these explosions work. While several lines of evidence indicate that the explosion is associated with the latest stages of stellar evolution of some massive stars and the collapse of their cores, the process in which the envelope is energetically ejected is poorly understood.

Recent extensive surveys and followup efforts are leading to the accumulation of large samples of well observed type II SNe. Given the diversity in the observed properties (e.g. peak luminosity), statistical inferences are likely to play an important role in improving our understanding of these events. Most observations of SNe in general, and type II in particular, consist of spectra and light curves of visible light acquired throughout weeks and months following the explosion. In order to connect the observed emission to the physical characteristics of the explosion and the progenitor star, studies usually either employ detailed radiation transfer calculations or use simplistic analytic models. While the former are more trustworthy, they are difficult to apply to the growing large samples of observed SNe, especially given the uncertainty in the late phase structure of the massive stars which are likely the progenitors. The application of simplistic analytic models is useful but may lead to crude errors in estimates of the interesting properties such as explosion energy, mass and radius of the progenitor.

Recently, we showed (Nakar et al. 2015; Katz et al. 2013) that the bolometric light curve can be used to extract information on the explosion which circumvents the difficulty of radiation transfer by direct use of energy conservation. For that we defined a time-weighted integrated luminosity (with the ^{56}Ni contribution subtracted) which is directly observable. We denoted it ET and in Nakar et al. (2015) measured it for a sample of 13 SNe. ET is set by the energetics of the explosion and the structure of the progenitor and it provides a direct relation between observations and explosion models which is simple, analytic and precise at the same time.

The purpose of this paper is to use hydrodynamic simulations to study the relation between this measurable quantity and useful parameters of the progenitor and explosion. To do that we calculate ET for a large set of 145 red supergiant models that are obtained by the stellar evolution code MESA (Paxton et al. 2011, 2013, 2015) by varying progenitor parameters on the main sequence (initial mass, metallicity and rotation) and an evolution parameter (mixing length parameter).

The paper is organized as follows. In section §2 we briefly repeat the arguments of Nakar et al. (2015) and Katz et al. (2013), and explain how the total radiation energy can be measured and how exactly it is connected to the hydrodynamic properties of the explosion. In section §3 we describe the set of numerical progenitors we

[1] The Raymond and Beverly Sackler School of Physics and Astronomy, Tel Aviv University, Tel Aviv 69978, Israel
[2] Racah Institute of Physics, The Hebrew University, Jerusalem 91904, Israel
[3] Particle Physics & Astrophysics Dept., Weizmann Institute of Science, Rehovot 76100, Israel

use and present the relations we find between ET and fundamental properties of the progenitor and explosion energy. In section §4 we use observations of SNe with measured ET and envelope velocity to constrain the envelope mass and radius, and SNe with measured ET, envelope velocity and pre-explosion radius to constrain the explosion energy.

2. ET IS MEASURABLE, INDEPENDENT OF RADIATION TRANSFER, AND SCALES AS VMR

We first briefly repeat the arguments of Nakar et al. (2015) and Katz et al. (2013). During the time span of about 1 to 10 days after the explosion, the expansion is homologous and the radiation is almost entirely trapped within the ejecta. In addition, the contribution of energy from the decay of ^{56}Ni is negligible. The total energy in radiation E_r, originating from the explosion shock wave, decreases with time adiabatically due to the work it does on the expanding ejecta. To a very good approximation it decreases in this phase as $E_r \propto 1/t$ where t is the time since explosion and thus we define

$$ET \equiv E_r t = \text{const} \qquad 1\text{d} \lesssim \text{t} \lesssim 10\text{d} \tag{1}$$

which is constant with time. Since there is negligible diffusion during this time, the quantity ET is completely set by the hydrodynamic properties of the explosion and is independent of the opacity of the ejecta. At later times diffusion becomes important and the trapped internal energy leaks out of the ejecta gradually to generate the observed luminosity. Thus, as shown by Nakar et al. (2015), by integrating over the observed bolometric luminosity (multiplied by t to compensate for adiabatic losses), and removing the contribution from ^{56}Ni, one can directly extract ET from observations.

To show that formally we start from the equation that describes the radiation energy which is trapped in the ejecta during the homologous phase:

$$\frac{dE_r(t)}{dt} = -\frac{E_r(t)}{t} + Q_{\rm Ni}(t) - L_{\rm bol}(t). \tag{2}$$

Here, $Q_{\rm Ni}(t)$ is the energy injection rate from ^{56}Ni decay and $L_{\rm bol}(t)$ is the bolometric luminosity. The term $-E_r/t$ is the total rate of adiabatic loss. After rearranging the equation, multiplying both sides by t and integrating over t in some interval $t_1 < t' < t_2$ we obtain

$$\int_{t_1}^{t_2} t'\, L_{\rm bol}(t')\, dt' = E_r(t_2)t_2 - E_r(t_1)t_1 + \int_{t_1}^{t_2} t'\, Q_{\rm Ni}(t')\, dt. \tag{3}$$

By choosing t_1 to be in the range $1\text{d} \lesssim \text{t} \lesssim 10\text{d}$, we can replace $E_r(t_1)t_1$ in equation 3 by ET. By choosing t_2 that is large enough (typically $\gtrsim 120$d) so the diffusion time is shorter than the expansion time and the remaining radiation in the ejecta is negligible, we can neglect the term $E_r(t_2)t_2$. Finally, since the (time weighted) integrated luminosity at early times is negligible, we can extend the integration from $t = 0$ without affecting the result. We therefore find

$$ET = \int_0^{t_2 \gtrsim 120\text{d}} t'\, (L_{\rm bol}(t') - Q_{\rm Ni}(t'))\, dt'. \tag{4}$$

The second term on the RHS of equation 4 can be calculated using

$$Q_{\rm Ni}(t) = \frac{M_{Ni}}{M_\odot}(6.45e^{-t_d/8.8} + 1.45e^{-t_d/111.3}) \times 10^{43} \text{erg s}^{-1} \tag{5}$$

where $t_d = t/\text{d}$ and M_{Ni} is the ^{56}Ni mass ejected in the explosion. M_{Ni} can be accurately inferred from the amplitude of the bolometric luminosity at late times $120\text{d} \lesssim \text{t} \lesssim 300\text{d}$ where to a very good approximation

$$L_{\rm bol}(t) = Q_{\rm Ni}(t) \qquad 120\text{d} \lesssim \text{t} \lesssim 300\text{d} \tag{6}$$

(at later times γ-ray escape may become significant). The value of ET can thus be directly extracted from observations of type II SNe using equations 4 - 6, as long as the bolometric luminosity is measured up to the ^{56}Ni tail phase (where $L_{\rm bol} = Q_{\rm Ni} \propto e^{-t_d/111.3}$).

We note that ET is also equal to the (time weighted) integrated 'cooling envelope luminosity' L_e defined as the luminosity that would have been generated if there was no ^{56}Ni present in the ejecta

$$ET = \int_0^\infty L_e(t) t dt. \tag{7}$$

Equation 7 is useful for studying the different approximations in radiation transfer simulations were the ^{56}Ni can be artificially extracted. This is demonstrated in figure 1 using the results of radiation transfer simulations reported in (Kasen & Woosley 2009).

We next derive the scaling we expect for ET with the progenitor radius, R_*, ejecta mass, $M_{\rm ej}$, and total explosion energy, $E_{\rm exp}$. In this paper we ignore the inner collapsing parts of the progenitor and the initial thermal and gravitational energy which is negligible when considering the material at large radii ($r \gtrsim 10^{10}$cm). The explosion is thus described as a shock wave traversing a cold standing star and a following expansion. While the shock is within the star, there is negligible diffusion and the thermal energy is dominated by radiation. Thus, for a set of progenitors with the same density profile[4], by the time the shock ends traversing the star and breaks out the radiation energy contained in the ejecta is $\propto E_{\rm exp}$ and the expansion time over which significant adiabatic losses take place is $\propto R_*/v_{\rm ej} \propto R_* E_{\rm exp}^{-1/2} M_{\rm ej}^{1/2}$. Thus for progenitors with similar profiles ET scales as

$$ET \propto E_{\rm exp}^{1/2} R_* M_{\rm ej}^{1/2} \propto \frac{E_{\rm exp} R_*}{v_{\rm ej}} \propto v_{\rm ej} R_* M_{\rm ej}, \tag{8}$$

where

$$v_{\rm ej} = \sqrt{2E_{\rm exp}/M_{\rm ej}} = \sqrt{\frac{\int v(m)^2 dm}{M_{\rm ej}}} \tag{9}$$

is the (mass weighted) RMS velocity of the ejecta ($v(m)$ is the velocity of the mass element dm). However, since stars with different initial conditions (e.g., ZAMS mass, metallicity, rotation, binarity, etc.) have different density

[4] Two progenitors, denoted as '1' and '2', have the same density profile if $\rho_1(r_1)\frac{R_{*,1}^3}{M_1} = \rho_2(r_2)\frac{R_{*,2}^3}{M_2}$, where ρ is density, M is the progenitor mass and $r_1 = r_2 \frac{R_{*,1}}{R_{*,2}}$

profiles before they explode, the coefficient in equation 8 for each progenitor structure is expected to be different. Below we calculate ET for a large set of progenitors and find the typical value of the coefficient and how it varies between different progenitors. We also study which of the progenitor and explosion properties can be constrained best by measuring ET.

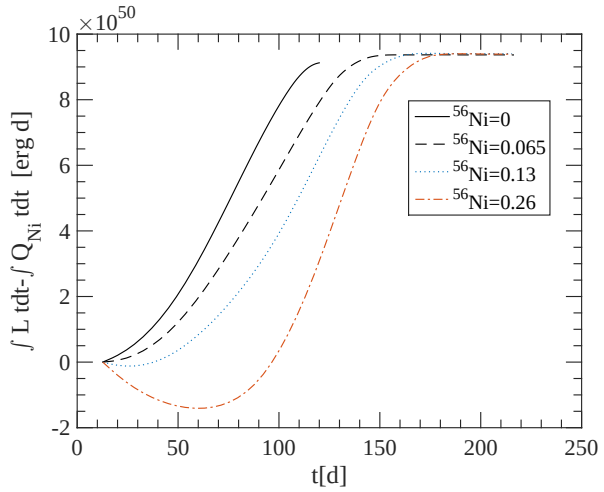

FIG. 1.— Synthetic ET extracted from the radiation transfer simulations of a type II SNe in figure 2 of Kasen & Woosley (2009). The value of ET is the asymptotic value of the curve $\int L_{\rm bol} tdt - \int Q_{\rm Ni} tdt$ shown as expressed in equations 4 & 5. The values of ^{56}Ni were taken from Kasen & Woosley (2009). As can be seen, the value of ET is independent of the amount of ^{56}Ni to an accuracy of a few percents.

3. NUMERICAL STUDY OF THE SCALING OF ET WITH PROGENITOR PARAMETERS

We have used the open source stellar evolution code MESA (Paxton et al. 2011, 2013, 2015) to calculate a large set of progenitors. Only single star evolution is considered (no binarity) and three initial conditions are varied - initial (ZAMS) mass (12-50 $M_\odot$), metallicity ($10^{-3} - 1$ z$_\odot$) and initial rotation (0-0.8 of breakup rotation rate). We have also varied one poorly constrained evolution parameter - the mixing length parameter (1.5-5). Altogether we calculate the stellar structure at the time of core collapse for 219 stars. Out of these 145 retain a hydrogen envelope at the time of explosion and are therefore considered here as plausible progenitors of type II SNe. Figure 2 depicts some of the main properties of these 145 progenitors. The evolution parameters, together with the main properties at explosion are given in table 2. More details on the set of progenitors we use here are given in Shussman et al. (2016)

In order to calculate ET for all the progenitors that retain hydrogen envelope, we excise the Si core from each progenitor (considered to be the explosion remnant), and explode it using a a simple 1D hydro-radiation code (see Shussman et al. 2016 for more details on the code). The explosion is induced by instantaneously releasing the explosion energy at the center of the ejecta. We then calculate ET, by extracting the asymptotic value of $E_r t$ at late times ($t = 100$ d) using hydrodynamics alone, without allowing for radiation to diffuse. We have verified that the results remain unchanged when radiation

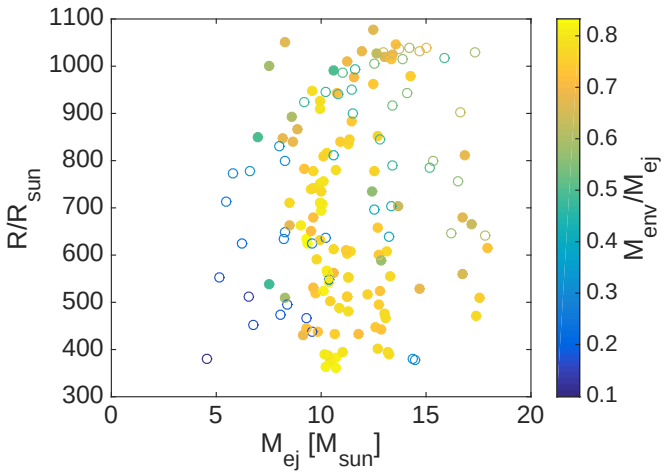

FIG. 2.— Properties of the numerical progenitors calculated via MESA. Plotted are the radius versus the ejecta mass (the remnant mass is irrelevant for our analysis). Different colors represent different values of the ratio between the envelope and ejecta mass. The filled circles represent progenitors with $M_{\rm ZAMS} \leq 20 M_\odot$, which seems to compose most (or all) of SNe II-P (Smartt 2015). The empty circles represent progenitors with $M_{\rm ZAMS} > 20 M_\odot$

transfer is included, in which case ET is calculated using equation 7. As explained above (equation 8) for a given progenitor we expect $ET \propto E_{\rm exp}^{1/2}$. We find that this is indeed the case in our simulations (to within 1%). Thus, as the dependence of ET on $E_{\rm exp}$ is known, we focus here on its dependence on the progenitor properties.

We first measure the coefficient of the scaling given in equation 8, in our progenitor sample. As can be seen in figure 3 for progenitors that retain most of their envelope, $M_{\rm env}/M_{\rm ej} > 0.6$, the relation

$$ET \approx 0.15 E_{\rm exp}^{1/2} R_* M_{\rm ej}^{1/2} = 0.2 \frac{E_{\rm exp} R_*}{v_{\rm ej}} = 0.1 v_{\rm ej} R_* M_{\rm ej} \quad (10)$$

is accurate to within about 30%. Such progenitors include almost all the models with initial mass $M_{\rm ZAMS} \leq 20\ M_\odot$ that have a massive envelope ($M_{\rm env} > 3\ M_\odot$). Pre-explosion images of progenitors and light curve modeling of type II-P SNe (e.g., Smartt 2015, and references therein) suggest that at least progenitors of this SN type fall into this category. Therefore equation 10 can be applied within fair accuracy to regular type II-P SNe.

Figure 3 also shows that although equation 10 is rather accurate for progenitors with $M_{\rm env}/M_{\rm ej} > 0.6$ it becomes less accurate as the envelope mass fraction drops, becoming inaccurate by more than an order of magnitude for $M_{\rm env}/M_{\rm ej} < 0.2$. To understand why low values of $M_{\rm env}/M_{\rm ej}$ affect the scaling of equation 10 we recall that ET is proportional to the *radiation* energy at the beginning of the homologous phase and not directly to the total explosion energy. In progenitors with low $M_{\rm env}/M_{\rm ej}$ most of the explosion energy is deposited in the core, but all the radiation energy deposited in the core is lost via adiabatic expansion well before the homologous phase. Only radiation energy deposited in the envelope remains by the beginning of the homologous phase. The total energy deposited in the envelope is roughly proportional

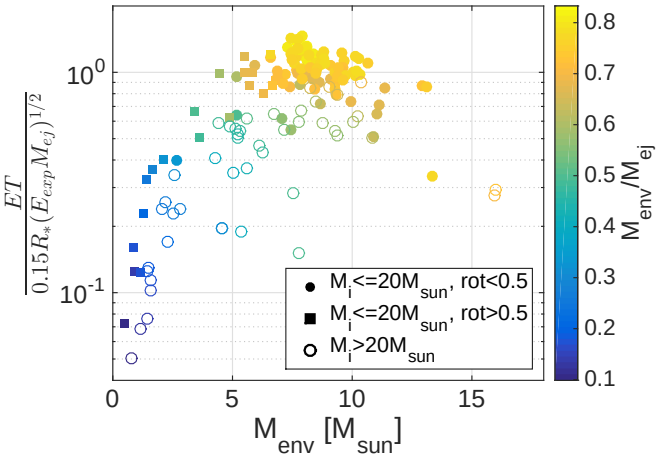

FIG. 3.— Ratio of ET and the estimator $E_{\rm exp}^{1/2}R_*M_{\rm ej}^{1/2}$ based on equation 8. *Empty circles* mark progenitors with $M_{\rm ZAMS} > 20M_\odot$. *Filled squares* mark fast rotating (> 0.5 of the breakout rate) progenitors with $M_{\rm ZAMS} < 20M_\odot$ and *filled circles* mark progenitors with $M_{\rm ZAMS} < 20M_\odot$ that are not fast rotating. As can be seen, the simple scaling of equation 8 captures the changes in ET in progenitors with $M_{\rm env}/M_{\rm ej} > 0.6$ but fails in progenitors that lost most of their envelope, either due to high initial mass or very fast rotation.

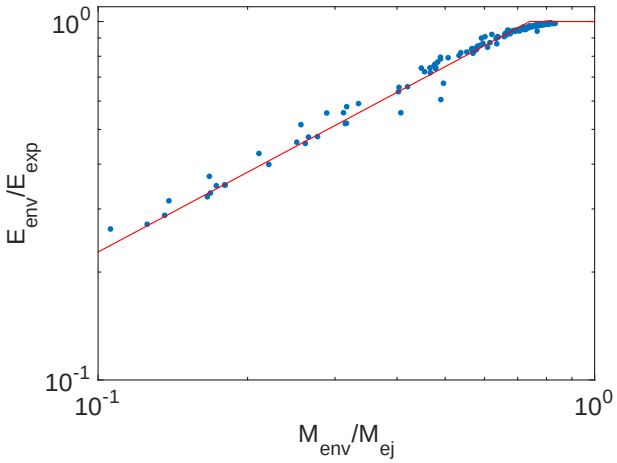

FIG. 4.— The fraction of the energy carried by the envelope out of the total explosion energy, $E_{\rm env}/E_{\rm exp}$, as a function of $M_{\rm env}/M_{\rm ej}$. The solid line is $min\{1.25(M_{\rm env}/M_{\rm ej})^{0.74}, 1\}$.

to $(M_{\rm env}/M_{\rm ej})^{-0.74}$, as can be seen in figure 4. Thus, a low value of $M_{\rm env}/M_{\rm ej}$ implies that a smaller fraction of the explosion energy contributes to ET.

In fact, the emission during the photospheric phase, after removing ^{56}Ni contribution, is completely dominated by the radiation energy deposited in the envelope during the SN explosion (hence the term 'cooling envelope emission'). Thus, ET, is actually a direct probe of the envelope properties and is not directly sensitive to properties of the core such as its mass or velocity. The same is true for any other probe that depends mostly on the cooling envelope emission (such as the photospheric velocity during the plateau, the plateau luminosity and duration, etc.). Therefore it is most useful to define scaling of ET

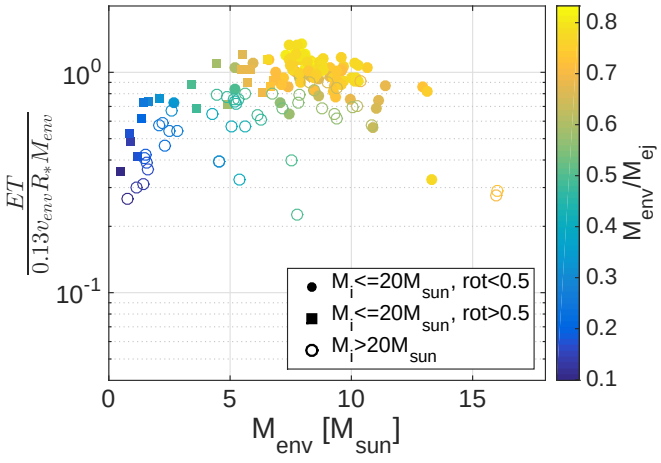

FIG. 5.— Relation between ET and the estimator $v_{\rm env}R_*M_{\rm env}$. Symbols are the same as in figure 3. This estimator, which depends on envelope properties only, shows a significant improvement over equation 10 for progenitors with low envelope mass, and moderate improvement for progenitors with massive envelopes. Still, for low mass envelope progenitors it is accurate only to within a factor of about 3.

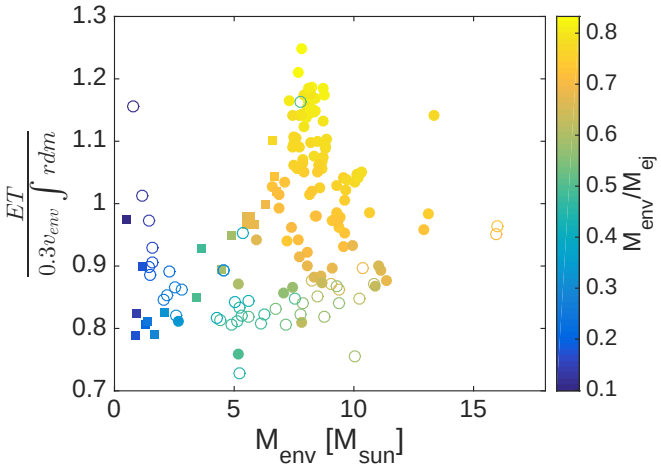

FIG. 6.— Relation between ET and the estimator $v_{\rm env}\int rdm$. Symbols are the same as in figure 3. This estimator is accurate to within 20% for all the progenitors in our sample.

that depends only on envelope properties:

$$ET \approx 0.18E_{\rm env}^{1/2}R_*M_{\rm env}^{1/2} = 0.26\frac{E_{\rm env}R_*}{v_{\rm env}} = 0.13v_{\rm env}R_*M_{\rm env}. \quad (11)$$

Here, $E_{\rm env}$ is the energy carried by the envelope to infinity and $v_{\rm env} = \sqrt{2E_{\rm env}/M_{\rm env}}$ is the envelope (mass weighted) RMS velocity. Figure 5 shows that indeed ET provides better estimates for global envelope properties than to those of the entire ejecta. Equation 11 provides a moderate improvement to progenitors that retain most of their envelope ($M_{\rm env}/M_{\rm ej} > 0.6$), where it is accurate to within about 20% (the normalization of equation 11 was chosen to better match such progenitors). More importantly, equation 11 is applicable also to progenitors that lost most of their envelope, where it is accurate to within a factor of about 3.

So far we have ignored the density structure of the envelope, which of course also affects the value of ET. When crossing a mass element, the shock deposits half of its energy as kinetic and half as internal (i.e., radiation). The expansion (and adiabatic cooling) of the element begins right after the shock crossing. Thus, the fraction of the deposited energy that remains once the homologous phase starts depends on the initial radius of each mass element and not directly on R_*. In both equations 10 and 11, R_* is used as the envelope radius. However, explosions of two progenitors with similar $v_{\rm env}$, $M_{\rm env}$, R_* and different density profiles will result in different values of ET. Specifically, ET will be lower in the progenitor that is more concentrated (i.e., most of its envelope mass is at a smaller radius). To account for that, one can attribute the initial radius to each mass element by replacing $M_{\rm env}R_*$ with the integral $\int rdm$. Note that the value of this integral is insensitive to whether it is taken over the envelope mass alone or over the entire ejecta since it is completely dominated by mass elements at large radii. Using this integral we find

$$ET \approx 0.3\ v_{\rm env} \int rdm = 0.3\ v_{\rm env}\overline{R}_{\rm env}M_{\rm env} = \\ = 0.42\ E_{\rm env}^{1/2}\overline{R}_{\rm env}M_{\rm env}^{1/2} = 0.6\ \frac{E_{\rm env}\overline{R}_{\rm env}}{v_{\rm env}}, \quad (12)$$

where

$$\overline{R}_{\rm env} = \frac{\int rdm}{M_{\rm env}} \quad (13)$$

is the mass weighted average radius of the envelope. Equation 12 is accurate to within about 20% to all the progenitors in our sample, as can be seen in Figure 6. Note that while $\int rdm$ hardly changes if the integral is performed over the entire progenitor including the core, $\overline{R}_{\rm env}$ does change due to the different mass in the denominator of equation 13.

4. SUPERNOVAE WITH SPECTRAL MEASUREMENT OF THE PHOTOSPHERIC VELOCITY

In many SNe spectral measurements provide information about the ejecta velocity. In particular for type II SNe, lines of Fe II and Sc II are considered to be good indicators of the photospheric velocity. In these SNe the photosphere crosses the H envelope from the outside in during the photospheric phase, providing a 'scan' of the envelope velocity range. The propagation of the photosphere at early time, before recombination becomes significant, depends only on the density and velocity profile of the ejecta and is relatively simple to model. Recombination becomes significant typically around day 20, when the photosphere has crossed only a very small fraction of the envelope ($< 0.1\ M_\odot$; see Shussman et al. 2016). The time at which the photosphere ends crossing the envelope is marked in type II SNe by a sharp drop in the luminosity and is observed typically around day 100. Thus, the photospheric velocity as measured around day 50, typically denoted v_{50}, provides a reasonable estimate of $v_{\rm env}$. Moreover, since the photospheric velocity evolves roughly as $t^{-0.5}$ (Nugent et al. 2006; Faran et al. 2014) it varies between day 20 and 100 by a factor of ≈ 2.2,

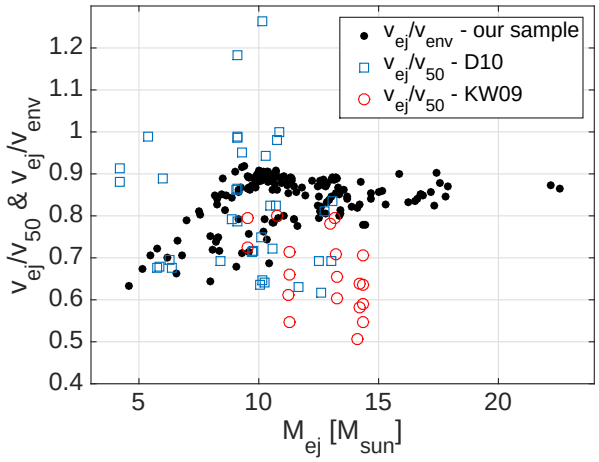

FIG. 7.— The ratio $v_{\rm ej}/v_{50}$ as found in the radiative-hydro simulations presented in Dessart et al. (2010) (*empty squares*) and Kasen & Woosley (2009) (*empty circles*). These are compared to the ratio $v_{\rm ej}/v_{\rm env}$ found in our numerical progenitors sample (*filled circles*).

implying that v_{50} estimates $v_{\rm env}$ to an accuracy of 50% at worst, and most likely much better.

The quality of v_{50} as an estimator of $v_{\rm env}$ can also be estimated from numerical modeling of type II SN light curves. For that we use the results of Dessart et al. (2010) (table 2 therein) and Kasen & Woosley (2009) (table 2 therein). Both studies present a set of hydrodynamic numerical SNe simulations that include detailed radiative transfer to explore properties of various observables including v_{50}. Unfortunately, these publications do not include the values of $v_{\rm env}$, but they do provide the values of $v_{\rm ej}$. Figure 7 depicts $v_{\rm ej}/v_{50}$ in Dessart et al. (2010) and Kasen & Woosley (2009), showing that they find in general $v_{\rm ej} \approx (0.8 \pm 0.2)v_{50}$. It also shows the values of $v_{\rm ej}/v_{\rm env}$ in our progenitor sample showing $v_{\rm ej} \approx (0.8 \pm 0.1)v_{\rm env}$. Thus, the reasonable assumption that $v_{\rm ej}/v_{\rm env}$ in our sample are similar to those of Dessart et al. (2010) and Kasen & Woosley (2009), implies that v_{50} is a good estimator of $v_{\rm env}$ and that at least in these simulations it is accurate to within about 25%.

Therefore, in SNe where both ET and v_{50} are measured we can estimate two interesting quantities based on equations 10 - 12. The first is $ET \cdot v_{50}$ which is an estimator of $E_{\rm exp}R_*$ (or more accurately of $E_{\rm env}R_*$). This can be used, for example, to estimate the explosion energy in cases where there are pre-explosion images of the progenitor, which constrain R_*. We have done that for six SNe for which ET, v_{50} and R_* are all measured independently (see table 1). Given that in all six the progenitor seems like normal red supergiants with initial masses $\lesssim 15\ M_\odot$ (Smartt 2015), equation 10 can probably be used to estimate $E_{\rm exp}$ within fair accuracy (within a factor of 2 given the large uncertainty in R_*). In figure 8 we depict $E_{\rm exp}$, as estimated based on equation 10 for these six SNe, as a function of the ^{56}Ni mass in the explosion. Even with that small number of SNe it is clear that $E_{\rm exp}$ varies by at least an order of magnitude between various SNe, and that SNe with $E_{\rm exp} \sim 2 \times 10^{50}$ erg are common (these SNe are also fainter and thus harder to detect, so their fraction of the total SNe volu-

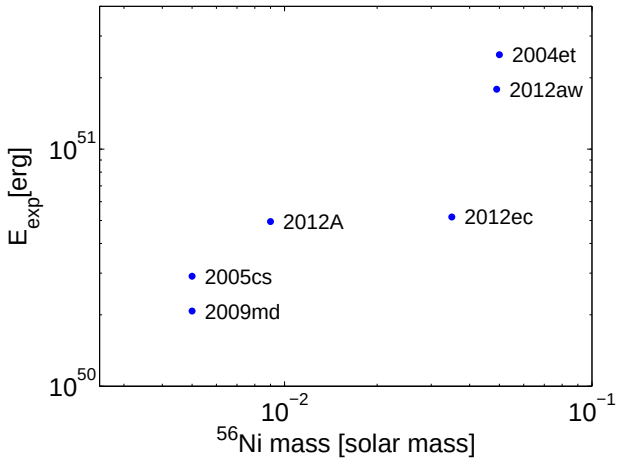

FIG. 8.— The explosion energy of six SNe for which ET, v_{50} and R_* are all measured independently, calculated using equation 10, plotted as a function of the ^{56}Ni mass in the explosion.

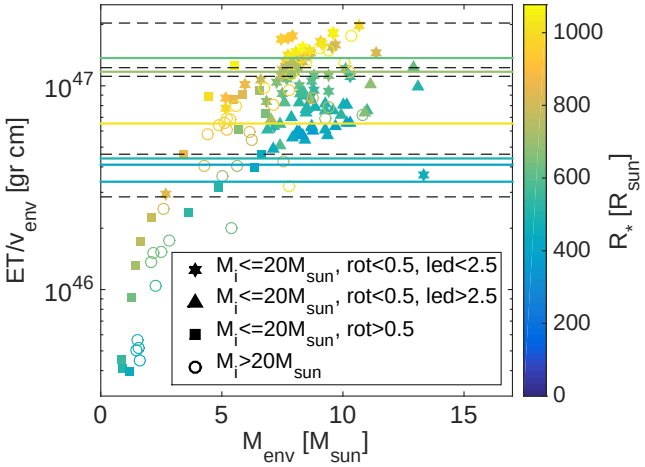

FIG. 9.— $ET/v_{\rm env}$ of all the numerically calculated progenitors in our sample as a function of $M_{\rm env}$ and color coded according to R_*. Progenitors are divided to four groups, based on their initial conditions. *Open circles*: massive ($M_{\rm ZAMS} > 20\ M_\odot$); *Filled rectangles*: fast rotating ($rot > 0.5$ of the breakout rotation rate and $M_{\rm ZAMS} <= 20\ M_\odot$); *filled triangles*: large mixing length parameter ($led > 2.5$, rotation lower than 0.5 breakout and $M_{\rm ZAMS} <= 20\ M_\odot$); *filled hexagons*: small mixing length parameter ($led < 2.5$, rotation lower than 0.5 breakout and $M_{\rm ZAMS} <= 20\ M_\odot$). Vertical lines are the ET/v_{50} values of the 11 SNe listed in table 1. Dashed lines for SNe without pre-explosion progenitor images and filled lines for SNe with pre-explosion images. For these the color line is color coded based on the progenitor radius as inferred from its luminosity and temperature in the pre-explosion image.

metric rate is probably higher than their representation in the observed sample). In addition, a strong, roughly linear, correlation exists between $E_{\rm exp}$ and the ^{56}Ni mass (Kushnir 2015). This correlation is most likely the main source of the well known correlation between the plateau luminosity, v_{50} and the ^{56}Ni mass (Hamuy 2003).

The second interesting quantity is ET/v_{50} which is an estimator of $ET/v_{\rm env} \propto M_{\rm env}R_*$. The main advantage of $ET/v_{\rm env}$ is that it is a property of the progenitor, namely it depends only on the progenitor structure, with no dependence on the explosion energy. Thus, we can compare the observed values of ET/v_{50} to the values of $ET/v_{\rm env}$ in our sample of numerical progenitors. This comparison is shown in figure 9, which depicts the observed values of the 11 SNe listed in table 1 as horizontal lines, solid for SNe with pre-explosion progenitor images and dashed for SNe without. It also shows all the values for our numerical progenitors, which are divided to four groups, each marked differently, according to the initial conditions. It can be seen that numerical progenitors that lost most of their envelope ($M_{\rm env} < 4\ M_\odot$) have $ET/v_{\rm env}$ that is lower than the observed ones. Almost all other numerical progenitors have $ET/v_{\rm env}$ within the observed range, but many are in the high end of that range ($1.5-2\cdot10^{47}$ gr cm) and few are in the low end ($0.25-0.5\cdot10^{47}$ gr cm). This is significant since half of the observed SNe in the sample have low values of $ET/v_{\rm env}$ and these are also the fainter ones, implying that they are most likely more abundant than their relative fraction in the sample.

A lower value of $ET/v_{\rm env}$ implies a lower value of $M_{\rm env}R_*$. In our numerical sample there are two groups for which $M_{\rm env}R_*$ is relatively small. One is the group of stars with small $M_{\rm env}$, which had lost a significant fraction of their envelope, either via fast rotation ($> 50\%$ of breakout velocity at birth) or due to a high initial mass ($> 20M_\odot$). However, this group does not seem to be the main origin of the observed low $ET/v_{\rm env}$ SNe. The reason for that is that high initial mass progenitors are not common (in all the cases where a progenitor was observed directly its mass was $< 20M_\odot$; Smartt 2015). Rotation, on the other hand, seems to need a fine tuning in order to lose just the correct amount of envelope mass (most of the fast rotating models lost too much of their mass while others did not lose enough). The second group of low $ET/v_{\rm env}$ progenitors are stars with smaller R_* ($\sim 400\ R_\odot$) due to a larger value of the mixing length parameter (3 or 5). Given the uncertainty in the value of this coefficient we consider this option as the more likely explanation for the large number of low $ET/v_{\rm env}$ SNe. This option is also supported by the measured radii of progenitors observed in pre-explosion images, where the three SNe with $ET/v_{\rm env} < 0.5$ in our sample with pre-explosion images have $R_* \approx 500\ R_\odot$. The result that many SNe progenitors have radii that are $\lesssim 500\ R_\odot$ is also supported by other, independent lines of evidence (Dessart et al. 2013; Davies et al. 2013; Gall et al. 2015; González-Gaitán et al. 2015)

5. CONCLUSIONS

We have used a large set of 145 numerical stars, calculated to the point of core collapse using the stellar evolution code MESA, in order to study the relation between the observable ET and SN progenitors. ET can be measured for any SN with observed bolometric light curve. It is a time weighted integral of the cooling envelope emission, with radioactive contribution removed, and it measures the amount of radiation energy that is deposited in the envelope at the beginning of the homologous phase. As such it constrains directly the structure of the progenitor and the explosion energy, without any dependence on radiation transfer physics or on the contribution of radioactive decay to the observed light.

We have found that although ET depends on the exact structure of the progenitor, it is an accurate probe

TABLE 1
SNe with measured ET and v_{50}

SN	ET [10^{55}erg s]	v_{50} [km/s]	L_{25} [10^{41}erg/s]	$R_*^\dagger$ [$R_\odot$]	Ref.
1999em	4	3280	14		1
1999gi	4.1	3700	16		1,2
2004et	5.5	4020	23	635	3
2005cs	0.86	1980	1.9	420	4
2007od	6.4	3130	32		5
2009N	1.2	2580	4.6		6
2009ib	0.88	3090	5.2		7
2009md	0.68	2000	2.4	471	8
2012A	1.2	2840	6.1	516	9
2012aw	4.6	3890	16	713	10
2012ec	2.2	3370	10	1031	11

1. Bersten & Hamuy (2009) 2. Leonard et al. (2002) 3. Maguire et al. (2010) 4. Pastorello et al. (2009) 5. Inserra et al. (2011) 6. Takáts et al. (2014) 7. Takáts et al. (2015) 8. Fraser et al. (2011) 9. Tomasella et al. (2013) 10. Dall'Ora et al. (2014) 11. Barbarino et al. (2015)

† Progenitor radius based on luminosity and effective temperature measured in pre-explosion images and listed in Smartt (2015). The reported errors in the measure luminosities and effective temperatures translate to errors of about 25%-50% in the radii.

A list of SNe with measured ET and v_{50} taken from Nakar et al. (2015). The light curves used to measure ET are reported in the listed references.

of $E_{\rm exp}^{1/2}R_*M_{\rm ej}^{1/2}$ for progenitors that retain most of the hydrogen envelope (equation 10). Specifically in our progenitor sample it is accurate to within 30% for progenitors with $M_{\rm env}/M_{\rm ej} > 0.6$. However, it is not an accurate probe of $E_{\rm exp}$ and $M_{\rm ej}$ for progenitors that lost most of their envelope, since ET is sensitive only to the fraction of the total energy that is deposited in the envelope, and this fraction is highly dependent on $M_{\rm env}/M_{\rm ej}$. We note that any observable which depends on the photospheric phase of type II SNe (e.g., plateau luminosity and duration), is sensitive mostly to envelope properties and is therefore, similarly to ET, only an approximate probe of the entire ejecta properties.

We have then explored how accurately ET can be related to envelope properties and found that it is a good probe of $E_{\rm env}^{1/2}R_*M_{\rm env}^{1/2} \propto v_{\rm env}R_*M_{\rm env}$ (equation 11). In our progenitor sample it is accurate to within 20% for progenitors with $M_{\rm env}/M_{\rm ej} > 0.6$ and up to a factor of three for progenitors that lost most of their envelope. The dependence on the envelope mass arises from the fact that progenitors that lost different fractions of their envelope mass have different density structures. We therefore consider a third combination of properties which takes the envelope structure into account, $v_{\rm env}\overline{R}_{\rm env}M_{\rm env}$, where $\overline{R}_{\rm env}$ is the mass weighted average radius of the envelope. In our sample ET measures $v_{\rm env}\overline{R}_{\rm env}M_{\rm env}$ to within 20% accuracy for all progenitors, regardless of their envelope mass.

When the bolometric light curve is accompanied by spectral measurements of line velocities then both ET and $v_{\rm env}$ can be estimated (as we have showed, v_{50} provides a good estimate for $v_{\rm env}$). This is very useful. First, the product $ET \cdot v_{50}$ is a probe of $E_{\rm exp}R_*$. We have used that in stars where R_* was measured from pre-explosion images to estimate $E_{\rm exp}$ in a robust way which is insensitive to detailed and uncertain light curve modeling. Second, the ratio ET/v_{50} depends on the progenitor structure only, and is independent of the explosion energy. We have compared this quantity as measured in 11 SNe to that of our sample of numerical progenitors. This comparison suggests that SNe progenitors often have a radius $R_* \lesssim 500\ R_\odot$, which is smaller than the typical RSG radius obtained by stellar evolution models. This result supports previous studies that got to the same conclusion based on completely different arguments (Dessart et al. 2010; Davies et al. 2013; González-Gaitán et al. 2015; Gall et al. 2015). Our simulations suggest that the small radii hint to relatively large values (3-5) of the mixing length parameter, as models with these values produce SNe with $ET/v_{\rm env}$ that is more similar to the observations.

We thank Dovi Poznanski for useful comments. This research was partially supported by the I-CORE Program (1829/12). TS and EN were partially supported by an ERC starting grant (GRB/SN), ISF grant (1277/13) and an ISA grant. BK was partially supported by the Beracha Foundation.

APPENDIX

The stellar evolution of the progenitor models was followed using the publicly available package MESA version 6596 (Paxton et al. 2011, 2013, 2015). To produce a wide range of progenitors, we varied the zero age main sequence (ZAMS) mass between $[10, 50]M_\odot$, the metallicity between $[2\times10^{-5}, 2\times10^{-2}]$, the mixing length parameter between $[1.5, 5]$, and the initial rotation rate between $[0, 0.8]$ of the breakup rotation rate. In all models, mass loss was determined

according to the "Dutch" recipe in MESA, combining the rates from Glebbeek et al. (2009); Nieuwenhuijzen & de Jager (1990); Nugis & Lamers (2000); Vink et al. (2001), with a coefficient $\eta = 1$, the convection was according to the Ledoux criterion, with a semi-convection efficiency parameter $\alpha_{sc} = 0.1$ (Paxton et al. 2013, eq. 12), and exponential overshoot with parameter $f = 0.008$ (Paxton et al. 2011, eq. 2).

The properties of the numerical progenitors are summarised in table 2. The initial (ZAMS) parameters are shown in rows 1-4, while the properties just before to the core collapse appear in rows 5-9. The key features of the explosion are given in rows 10-11, and are normalized to be independent of the explosion energy. We denote $E_{\rm exp,51} = E_{\rm exp}/10^{51}$erg.

TABLE 2
Initial parameters and properties of the numerical progenitors

M_{ZAMS} $[M_\odot]$	Z	mixing length parameter	rotation [breakup]	$M_{\rm final}$ $[M_\odot]$	$M_{\rm ej}$ $[M_\odot]$	$M_{\rm env}$ $[M_\odot]$	R_* $[R_\odot]$	$\overline{R}_{\rm env}$ $[R_\odot]$	$E_{\rm env}/E_{\rm exp}$	$ET/E_{\rm exp,51}^{1/2}$ $[10^{55}$erg s]
11	0.02	2	0.4	10.07	9.72	7.19	518	225	0.97	2.34
12	0.0002	1.5	0	12.94	11.39	8.82	608	280	0.98	3.76
12	0.0002	1.5	0.2	12.89	11.27	8.72	603	271	0.98	3.56
12	0.0002	2	0	12.93	11.31	8.80	553	237	0.98	3.19
12	0.0002	2	0.2	12.88	11.28	8.68	552	230	0.98	2.99
12	0.0002	2	0.4	12.89	11.19	8.25	609	262	0.97	3.16
12	0.0002	3	0	12.94	11.31	8.85	480	193	0.98	2.63
12	0.0002	3	0.2	12.93	11.25	8.54	512	205	0.97	2.63
12	0.0002	3	0.4	12.89	11.25	8.46	511	200	0.97	2.51
12	0.002	1.5	0	11.59	10.02	7.70	736	353	0.98	4.43
12	0.002	1.5	0.2	10.49	8.86	5.94	867	438	0.95	4.09
12	0.002	1.5	0.4	10.80	9.17	6.60	783	379	0.97	4.10
12	0.002	2	0	12.23	10.59	8.20	614	270	0.98	3.51
12	0.002	2	0.2	11.60	9.94	7.49	633	279	0.97	3.35
12	0.002	2	0.4	11.32	9.64	6.86	681	298	0.96	3.16
12	0.002	3	0	12.48	10.85	8.47	489	198	0.98	2.63
12	0.002	3	0.2	11.98	10.41	7.85	502	201	0.97	2.48
12	0.002	3	0.4	11.25	9.60	6.89	532	210	0.96	2.29
12	0.002	5	0	12.66	11.02	8.72	396	153	0.99	2.12
12	0.002	5	0.2	11.48	9.86	7.12	438	161	0.96	1.82
12	0.002	5	0.4	12.23	10.65	7.90	432	161	0.97	1.96
12	0.02	1.5	0	11.51	9.97	7.93	910	454	0.98	6.22
12	0.02	1.5	0.2	11.36	9.93	7.74	926	466	0.98	6.13
12	0.02	1.5	0.4	11.16	9.59	7.45	948	481	0.98	6.20
12	0.02	1.5	0.6	9.93	8.26	5.52	1052	563	0.95	5.27
12	0.02	2	0	11.70	10.07	8.08	709	319	0.98	4.30
12	0.02	2	0.2	11.49	9.92	7.84	752	337	0.98	4.47
12	0.02	2	0.4	11.23	9.65	7.48	778	350	0.98	4.38
12	0.02	2	0.6	10.29	8.65	5.84	841	387	0.94	3.66
12	0.02	2	0.8	7.41	5.49	1.41	714	278	0.52	0.80
12	0.02	3	0	11.92	10.34	8.36	559	229	0.99	3.22
12	0.02	3	0.2	11.86	10.27	8.23	568	232	0.99	3.19
12	0.02	3	0.4	11.41	9.81	7.60	592	238	0.98	3.00
12	0.02	3	0.6	11.19	9.53	6.78	650	253	0.95	2.74
12	0.02	3	0.8	7.16	5.17	0.87	553	160	0.37	0.30
12	0.02	5	0	12.27	10.70	8.70	383	149	0.99	2.16
12	0.02	5	0.2	11.87	10.31	8.19	388	148	0.99	2.07
12	0.02	5	0.4	11.78	10.16	8.11	390	149	0.99	2.08
12	0.02	5	0.6	11.00	9.27	6.66	445	159	0.96	1.75
12	0.02	5	0.8	10.08	8.27	4.87	510	166	0.86	1.35
13	0.02	2	0	11.71	10.00	8.11	708	318	0.98	4.37
13	0.02	2	0.2	11.56	9.95	7.91	711	318	0.98	4.17
13	0.02	2	0.4	11.26	9.53	7.48	739	333	0.98	4.13
13	0.02	2	0.6	10.01	8.18	5.50	847	389	0.93	3.56
14	0.02	2	0	12.34	10.68	8.33	780	354	0.98	4.55
14	0.02	2	0.2	12.04	10.28	7.89	817	375	0.97	4.66
14	0.02	2	0.6	8.94	6.98	3.41	851	380	0.79	2.21
15	2e-05	1.5	0	14.98	13.27	10.29	555	247	0.98	3.44
15	2e-05	1.5	0.4	14.76	12.74	9.40	601	250	0.96	3.03
15	2e-05	3	0	14.97	13.07	10.18	465	182	0.98	2.51
15	2e-05	3	0.4	14.91	12.77	9.59	496	188	0.97	2.41
15	2e-05	5	0	14.98	13.22	10.30	390	146	0.98	2.05
15	2e-05	5	0.4	14.90	12.85	9.35	442	152	0.95	1.84
15	0.0002	1.5	0	14.95	13.10	10.13	608	277	0.98	3.82
15	0.0002	1.5	0.4	14.77	12.70	9.40	658	295	0.97	3.65
15	0.0002	3	0	14.92	13.02	10.02	476	188	0.98	2.55
15	0.0002	3	0.4	14.83	12.79	9.29	524	201	0.96	2.46
15	0.0002	5	0	14.93	13.16	10.14	394	149	0.98	2.06
15	0.0002	5	0.4	14.79	12.60	9.27	448	161	0.96	1.97
15	0.002	1.5	0	14.27	12.53	9.56	778	376	0.98	5.02
15	0.002	1.5	0.4	10.37	8.62	5.18	894	466	0.91	3.69
15	0.002	3	0	14.10	12.21	9.28	518	207	0.97	2.68
15	0.002	3	0.4	12.62	10.58	7.41	562	219	0.94	2.33
15	0.002	5	0	14.44	12.68	9.69	401	152	0.98	2.03

TABLE 2 — *Continued*

M_{ZAMS} $[M_\odot]$	Z	mixing length parameter	rotation [breakup]	$M_{\rm final}$ $[M_\odot]$	$M_{\rm ej}$ $[M_\odot]$	$M_{\rm env}$ $[M_\odot]$	R_* $[R_\odot]$	$\overline{R}_{\rm env}$ $[R_\odot]$	$E_{\rm env}/E_{\rm exp}$	$ET/E_{\rm exp,51}^{1/2}$ $[10^{55}$erg s]
15	0.002	5	0.4	13.63	11.79	8.45	432	158	0.95	1.84
15	0.02	2	0	13.05	11.27	8.68	835	382	0.97	4.91
15	0.02	2	0.2	12.66	10.94	8.17	841	383	0.97	4.57
15	0.02	2	0.4	13.15	11.37	8.60	845	385	0.97	4.77
15	0.02	2	0.6	7.84	5.77	1.67	773	314	0.56	1.00
16	0.02	2	0	14.47	12.68	9.67	851	385	0.97	5.05
16	0.02	2	0.2	13.25	11.47	8.38	883	404	0.96	4.70
16	0.02	2	0.4	12.71	10.78	7.66	943	440	0.96	4.69
16	0.02	2	0.6	8.62	6.62	2.10	777	313	0.58	1.19
17	0.02	2	0	14.25	12.47	9.10	963	451	0.96	5.43
17	0.02	2	0.2	13.44	11.59	8.07	977	456	0.95	4.87
17	0.02	2	0.4	13.19	11.25	7.73	1009	480	0.94	4.96
17	0.02	2	0.6	8.50	6.20	1.31	625	208	0.43	0.53
18	0.02	2	0	16.25	14.23	10.67	978	451	0.97	5.98
18	0.02	2	0.2	15.22	13.32	9.61	1015	478	0.96	5.78
18	0.02	2	0.4	13.89	11.93	8.06	1031	489	0.94	5.06
18	0.02	2	0.6	8.58	6.57	0.91	512	131	0.32	0.24
19	0.02	2	0	15.46	13.53	9.58	1046	491	0.95	5.78
19	0.02	2	0.2	14.47	12.50	8.34	1077	509	0.93	5.23
19	0.02	2	0.6	9.42	6.78	1.17	452	90	0.35	0.22
20	2e-05	3	0.4	17.88	17.17	10.91	666	187	0.87	2.08
20	0.0002	1.5	0	19.94	17.41	13.33	471	58	0.94	0.98
20	0.0002	1.5	0.4	19.48	16.86	11.38	812	349	0.94	4.18
20	0.0002	3	0	19.91	17.90	12.93	616	238	0.96	3.35
20	0.0002	3	0.4	19.45	16.76	11.12	680	245	0.92	2.92
20	0.0002	5	0	19.92	17.57	13.11	511	185	0.97	2.71
20	0.0002	5	0.4	19.38	16.76	11.02	561	184	0.91	2.19
20	0.002	1.5	0	14.69	12.62	7.83	1027	522	0.92	4.74
20	0.002	1.5	0.4	12.73	10.59	5.18	991	472	0.80	3.05
20	0.002	3	0	15.70	13.67	8.65	703	271	0.90	2.76
20	0.002	3	0.4	14.72	12.44	7.04	735	271	0.83	2.36
20	0.002	5	0	16.70	14.69	9.94	529	186	0.92	2.20
20	0.02	2	0	15.41	13.38	9.11	1025	472	0.94	5.18
20	0.02	2	0.2	15.00	13.02	8.63	1019	469	0.93	4.91
20	0.02	2	0.4	10.10	8.00	2.68	830	325	0.59	1.39
21	0.02	2	0	15.74	13.70	9.04	1037	465	0.92	4.90
21	0.02	2	0.2	14.98	12.95	8.26	1030	461	0.91	4.63
21	0.02	2	0.4	11.47	9.18	4.43	925	389	0.77	2.44
22	0.02	2	0	17.37	15.01	10.36	1039	456	0.94	5.33
22	0.02	2	0.2	10.56	8.29	2.59	799	283	0.56	1.17
22	0.02	2	0.4	12.31	10.23	4.88	945	392	0.76	2.55
22	0.02	2	0.6	10.73	8.07	1.45	473	92	0.35	0.25
23	0.02	2	0	16.80	14.70	9.40	1032	442	0.90	4.65
23	0.02	2	0.2	13.09	11.04	5.60	986	417	0.79	3.01
23	0.02	2	0.4	12.94	10.80	5.13	942	380	0.75	2.54
23	0.02	2	0.6	10.49	7.96	0.79	153	15	0.24	0.03
24	0.02	2	0	16.32	14.22	8.47	1040	440	0.87	4.26
24	0.02	2	0.2	14.63	12.55	6.75	1005	418	0.82	3.42
24	0.02	2	0.4	10.67	8.24	2.07	634	187	0.46	0.65
25	2e-05	1.5	0	24.97	22.17	16.01	154	20	0.95	0.31
25	2e-05	1.5	0.4	19.00	15.87	7.78	1018	86	0.61	0.91
25	0.0002	3	0.4	18.33	15.18	7.53	784	160	0.67	1.28
25	0.0002	5	0	24.90	22.58	15.95	149	19	0.94	0.29
25	0.0002	5	0.4	16.20	13.22	5.38	639	94	0.56	0.65
25	0.002	1.5	0	14.30	11.63	5.21	994	436	0.74	2.61
25	0.002	1.5	0.4	20.00	17.31	10.06	1030	409	0.85	3.77
25	0.002	3	0	17.94	15.31	8.78	799	292	0.84	2.71
25	0.002	3	0.4	19.40	16.51	9.39	756	240	0.82	2.33
25	0.002	5	0	18.44	16.22	9.29	646	208	0.83	2.09
25	0.002	5	0.4	20.54	17.79	10.83	640	183	0.85	2.01
25	0.02	2	0	16.08	13.89	7.86	1016	416	0.84	3.76
25	0.02	2	0.2	13.62	11.46	5.34	950	378	0.74	2.59
25	0.02	2	0.4	11.03	8.27	2.19	649	194	0.48	0.71
25	0.02	2	0.6	11.60	9.05	1.14	260	34	0.27	0.08
26	0.02	2	0	16.45	14.10	7.79	943	360	0.82	3.14
26	0.02	2	0.2	13.88	11.49	5.22	900	338	0.72	2.29
26	0.02	2	0.4	11.10	8.38	1.51	495	103	0.35	0.28
27	0.02	2	0	16.22	13.38	7.14	917	337	0.80	2.71
27	0.02	2	0.2	13.37	10.61	4.28	811	278	0.66	1.59
27	0.02	2	0.4	12.36	9.59	2.51	625	169	0.46	0.65
28	0.02	2	0	15.66	12.81	6.12	844	288	0.74	2.07
28	0.02	2	0.2	19.53	16.63	10.24	902	325	0.87	3.44
28	0.02	2	0.4	11.86	9.30	1.57	467	87	0.33	0.24
29	0.02	2	0	16.21	13.40	6.25	790	254	0.72	1.85
29	0.02	2	0.2	12.94	10.22	2.83	638	173	0.48	0.72

TABLE 2 — *Continued*

M_{ZAMS} $[M_\odot]$	Z	mixing length parameter	rotation [breakup]	$M_{\rm final}$ $[M_\odot]$	$M_{\rm ej}$ $[M_\odot]$	$M_{\rm env}$ $[M_\odot]$	R_* $[R_\odot]$	$\overline{R}_{\rm env}$ $[R_\odot]$	$E_{\rm env}/E_{\rm exp}$	$ET/E_{\rm exp,51}^{1/2}$ $[10^{55}$erg s]
29	0.02	2	0.4	12.94	10.36	2.29	548	124	0.40	0.44
30	0.02	2	0	16.05	13.37	5.62	703	205	0.66	1.39
30	0.02	2	0.2	15.34	12.52	5.04	697	203	0.64	1.28
30	0.02	2	0.4	12.94	10.45	1.42	275	38	0.29	0.10
35	0.02	2	0	17.11	14.47	4.55	377	72	0.52	0.41
35	0.02	2	0.2	17.10	14.37	4.55	380	73	0.52	0.42

REFERENCES

Barbarino, C., Dall'Ora, M., Botticella, M. T., et al. 2015, MNRAS, 448, 2312
Bersten, M. C., & Hamuy, M. 2009, ApJ, 701, 200
Dall'Ora, M., Botticella, M. T., Pumo, M. L., et al. 2014, ApJ, 787, 139
Davies, B., Kudritzki, R.-P., Plez, B., et al. 2013, ApJ, 767, 3
Dessart, L., Hillier, D. J., Waldman, R., & Livne, E. 2013, MNRAS, 433, 1745
Dessart, L., Livne, E., & Waldman, R. 2010, MNRAS, 408, 827
Faran, T., Poznanski, D., Filippenko, A. V., et al. 2014, MNRAS, 442, 844
Fraser, M., Ergon, M., Eldridge, J. J., et al. 2011, MNRAS, 417, 1417
Gall, E. E. E., Polshaw, J., Kotak, R., et al. 2015, A&A, 582, A3
Glebbeek, E., Gaburov, E., de Mink, S. E., Pols, O. R., & Portegies Zwart, S. F. 2009, A&A, 497, 255
González-Gaitán, S., Tominaga, N., Molina, J., et al. 2015, MNRAS, 451, 2212
Hamuy, M. 2003, ApJ, 582, 905
Inserra, C., Turatto, M., Pastorello, A., et al. 2011, MNRAS, 417, 261
Kasen, D., & Woosley, S. E. 2009, ApJ, 703, 2205
Katz, B., Kushnir, D., & Dong, S. 2013, ArXiv e-prints, arXiv:1301.6766
Kushnir, D. 2015, ArXiv e-prints, arXiv:1506.02655
Leonard, D. C., Filippenko, A. V., Li, W., et al. 2002, AJ, 124, 2490
Maguire, K., Di Carlo, E., Smartt, S. J., et al. 2010, MNRAS, 404, 981
Nakar, E., Poznanski, D., & Katz, B. 2015, ArXiv e-prints, arXiv:1506.07185
Nieuwenhuijzen, H., & de Jager, C. 1990, A&A, 231, 134
Nugent, P., Sullivan, M., Ellis, R., et al. 2006, ApJ, 645, 841
Nugis, T., & Lamers, H. J. G. L. M. 2000, A&A, 360, 227
Pastorello, A., Valenti, S., Zampieri, L., et al. 2009, MNRAS, 394, 2266
Paxton, B., Bildsten, L., Dotter, A., et al. 2011, ApJS, 192, 3
Paxton, B., Cantiello, M., Arras, P., et al. 2013, ApJS, 208, 4
Paxton, B., Marchant, P., Schwab, J., et al. 2015, ApJS, 220, 15
Shussman, T., Waldman, R., & Nakar, E. 2016, in preperation
Smartt, S. J. 2015, PASA, 32, e016
Takáts, K., Pumo, M. L., Elias-Rosa, N., et al. 2014, MNRAS, 438, 368
Takáts, K., Pignata, G., Pumo, M. L., et al. 2015, MNRAS, 450, 3137
Tomasella, L., Cappellaro, E., Fraser, M., et al. 2013, MNRAS, 434, 1636
Vink, J. S., de Koter, A., & Lamers, H. J. G. L. M. 2001, A&A, 369, 574